arXiv:1404.4520v2 [cond-mat.mes-hall] 22 Apr 2014

Goos-Hänchen like Shifts for Graphene Barrier in Constant Magnetic Field

Ahmed Jellal[*a,b], **Miloud Mekkaoui**[b], and **Youness Zahidi**[b]

[a] *Saudi Center for Theoretical Physics, Dhahran, Saudi Arabia*
[b] *Theoretical Physics Group, Faculty of Sciences, Chouaïb Doukkali University, PO Box 20, 24000 El Jadida, Morocco*

Abstract

We consider a system of Dirac fermions in graphene submitted to a constant perpendicular magnetic field and scattered by a barrier potential. We show that our system can be used to establish a link with quantum optics through the Goos-Hänchen shifts. This can be done by evaluating the corresponding transmission probability and shift phase. We obtain Goos-Hänchen like shifts in terms of different physical parameters such as energy, electrostatic potential strength and magnetic field. On the light of this relation, we discuss the obtained results and make comparison with literature.

PACS numbers: 72.80.Vp, 73.21.-b, 71.10.Pm, 03.65.Pm
Keywords: Graphene, magnetic field, transmission, barrier potential, Goos-Hänchen shifts.

[*] ajellal@ictp.it – a.jellal@ucd.ac.ma

1 Introduction

Graphene [1,2], a single sheet of carbon honeycomb, has ignited intense research activities to elucidate its electronic properties. The linear energy dispersion relation of the charge carriers, near the Dirac point in the electronic band structure, make charge transport in graphene substantially different from that of conventional two-dimensional (2D) electronic systems [3,4]. What makes graphene so attractive for research is that the spectrum closely resembles the Dirac spectrum for massless fermions [5, 6]. The charge carriers are described as massless, chiral relativistic fermions, governed by the Dirac equation. Their relativistic behavior lead to one of its fascinating properties is the so-called Klein tunneling [7]. These properties are what enable graphene to break so many records in terms of strength, electricity and heat conduction as well as many others. Electronic confinement has been demonstrated in graphene microstructures using standard lithography methods [8], which makes the fabrication of resonant-tunneling structures based on graphene practicable.

On the other hand, the Goos-Hänchen (GH) effect [9] is a phenomenon that originated in classical optics in which a light beam reflecting off a surface is spatially shifted as if it had briefly penetrated the surface before bouncing back. The interface has to separate different dielectric materials (such as glass or water), and absorption or transmission should be small enough to allow a substantial reflected beam to form [10]. The size of the GH effect is proportional to the derivative of the refection phase with respect to the angle of incidence. In addition to shifting beam position, the GH effect can manifest itself in alterations of differential cross sections [11] of laser mode dynamics [12] and of mode spectra [13].

During the few past years there is a progress in studying transport properties for charge carriers in graphene through single or double magnetic barrier in combination with gate voltage induced electrostatic potential. Among these transport properties we cite the quantum version of the GH effect originating from the reflection of particles from interfaces. Beenakker *et al.* [14] have pioneered the quantum GH effect at the p-n interface in graphene. Many works in various graphene-based nanostructures, including single [15], double barrier [16, 17], and superlattices [18], showed that the Goos-Hänchen like (GHL) shifts can be enhanced by the transmission resonances and controlled by varying the electrostatic potential and induced gap [15]. Similar to those in semiconductors, the GH shifts in graphene can also be modulated by electric and magnetic barriers [19], which influences the electronic transport in graphene-based electronics. Also we mention that the gate-controlled density of both p and n carrier types in graphene was used to demonstrate the electronic analogue of fibre-optic guiding [20].

Very recently, the GHL shifts for Dirac fermions in graphene scattered by double barrier structures have been studied in [17]. After obtaining the solution for the energy spectrum, the boundary conditions have been used to explicitly determine GHL shifts and the associated transmission probability. These two quantities have been analyzed at resonances by studying their main characteristics as a function of the energy and electrostatic potential parameters. To check the validity of the computations done in [17], the previous results have been recovered for a single barrier [15] under appropriate limits and considerations.

Motivated by different developments on the subject and in particular [15–17], we investigate the GHL shifts for a system made of graphene with gap in presence of constant magnetic field, single

barrier potential and Zeeman effect. By splitting our system into three regions, we determine the solutions of the energy spectrum in terms of different physical quantities. After matching the wave functions at both interfaces of potential width, we calculate the transmission coefficient as well as the GHL shifts. To give a better understanding of our results, we plot different figures versus physical parameters entering in the game and underline their behaviors.

The present paper is organized as follows. In section 2, we formulate our problem to include different part in the Hamiltonian system describing particles scattered by graphene barrier in external magnetic field. We obtain the solution of the energy spectrum corresponding to each region in terms of different scattering parameters. In section 3 the scattering problem for Dirac fermions will be solved, by using the boundary condition, in order to calculate the transmission coefficient and their phase. In section 4, we analyze the GHL shift and the transmission and we discuss our results by presenting different plot. Finally, we conclude our results and present some discussions.

2 Theoretical model

We consider a system of massless Dirac fermions through a strip of graphene with the Fermi energy E and the incidence angle ϕ_0 with respect to the x-direction of the potential barrier. This system is split into three regions denoted by 1, 2, 3 and each region is characterized by the corresponding potential and interaction with external sources according to Figure 1:

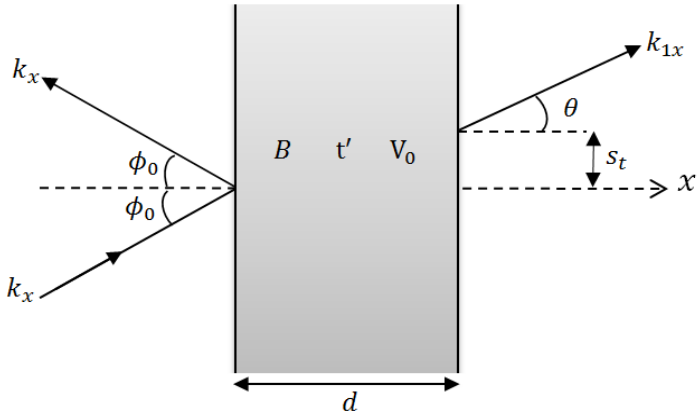

Figure 1: Schematic diagram for the monolayer graphene barriers with different physical parameters.

The potential barrier has a rectangular shape

$$V(x) = \begin{cases} V_0, & 0 < x < d \\ 0, & \text{otherwise} \end{cases} \tag{1}$$

which is infinite along the y-direction. In the barrier region of zero gap, both up-spin and down-spin carriers obey the Dirac equation of motion described by the Hamiltonian

$$H_0 = -i\hbar v_F \sigma \cdot \nabla \tag{2}$$

with the linear dispersion relation $E = \hbar \epsilon v_F$ where $v_F \approx 10^6 ms^{-1}$ is the Fermi velocity and $\sigma = (\sigma_x, \sigma_y)$ represents the Pauli matrices. In the central part of the sheet, we introduce an external

magnetic field $B_\circ\hat{z}$, perpendicular to the graphene sheet, along the z-direction defined by

$$B(x,y) = B_0\Theta(dx - x^2) \tag{3}$$

where Θ is the Heaviside step function. We also include the effect of Zeeman splitting, that is characterized by an energy gap 2Δ. Choosing the Landau gauge and imposing continuity of the vector potential at the boundary to avoid nonphysical effects, the corresponding vector potential $A(x,y) = (0, A_y(x))$ created by the magnetic field, takes the form

$$A_y(x) = \frac{c}{el_B^2}\begin{cases} 0, & x < 0 \\ x, & 0 \le x \le d \\ d, & x > d \end{cases} \tag{4}$$

where $l_B = \sqrt{c/eB_0}$ is the magnetic length, c being the speed of light and e the electronic charge. After defining the potential parameters relevant to all regions, we can write the Hamiltonian for one-pseudospin component describing our system as

$$H_\tau = v_F\vec{\sigma}\cdot\left(-i\hbar\vec{\nabla} + \frac{e}{c}\vec{A}(x,y)\right) + \Delta\sigma_z + V(x) + \frac{\tau}{2}g\mu_B B(x,y) \tag{5}$$

where $\tau = 1$ for up spin and $\tau = -1$ for down spin, the energy gap is defined by

$$\Delta = t^{'}\Theta(dx - x^2) \tag{6}$$

the spin g-factor (assumed to be 2) [21] of the carriers and μ_B represents the Bohr magneton. Last term in (5) is due to the Zeeman effect.

In order to solve the eigenvalue equation $H_\tau\psi = \epsilon\psi$ (in the unit system $\hbar = c = e = 1$), we can separate variables and write the eigenspinors as $\psi(x,y) = \varphi(x)\chi(y)$. We notice that the momentum along the y-direction is conserved, which allows us to write the eigenspinors as follows

$$\psi(x,y) = \varphi(x)e^{\tau ik_y y}. \tag{7}$$

Then in region 1, we end up with the upper and lower components of the eignespinor of the incident and reflection waves

$$\psi_1(x,y) = \begin{pmatrix} 1 \\ \alpha \end{pmatrix} e^{ik_x x}e^{\tau ik_y y} + r_\tau \begin{pmatrix} 1 \\ -\alpha^{-1} \end{pmatrix} e^{-ik_x x}e^{\tau ik_y y} \tag{8}$$

where the complex parameter is

$$\alpha = s_0\frac{k_x + ik_y}{\sqrt{k_x^2 + k_y^2}} = s_0 e^{\mathbf{i}\phi}$$

and $s_0 = \mathsf{sgn}(\epsilon)$ refers to the conduction and valence bands and ϕ is the angle that incident electrons make with the x-direction, see Figure 1. The x- and y-components of the electron wave vector, respectively, read as

$$k_x = \epsilon\cos\phi, \qquad k_y = \epsilon\sin\phi \tag{9}$$

which give the dispersion relation

$$\epsilon = s_0\sqrt{k_x^2 + k_y^2}. \tag{10}$$

In similar way to the above study, we can show that the wave function in the transmitted region 3 can be expressed as

$$\psi_3(x,y) = t_\tau \begin{pmatrix} 1 \\ \beta \end{pmatrix} e^{ik_{1x}x} e^{\tau i k_y y} \tag{11}$$

where we have introduced the perpendicular and parallel components of the wave vector as

$$k_{1x} = \epsilon \cos\theta, \qquad k_y = \epsilon \sin\theta - \frac{d}{l_B^2} \tag{12}$$

and the parameter β is

$$\beta = s_0 \frac{k_{1x} + i\left(k_y + \frac{d}{l_B^2}\right)}{\sqrt{k_{1x}^2 + \left(k_y + \frac{d}{l_B^2}\right)^2}} = s_0 e^{i\theta} \tag{13}$$

with the phase $\theta = \arctan\left(\frac{k_y + d/l_B^2}{k_{1x}}\right)$. It is clearly seen that the dispersion relation takes the form

$$\epsilon = s_0 \sqrt{k_{1x}^2 + \left(k_y + \frac{d}{l_B^2}\right)^2}. \tag{14}$$

Now we can establish a connection between the two angles. This can fixed by exploiting conservation of the momentum p_y to end up with

$$\sin\theta = \sin\phi + \frac{d}{\epsilon l_B^2}. \tag{15}$$

This will play a crucial role in the forthcoming analysis and especially when we deal with the transmission and GH shifts.

To find all solutions of the energy spectrum, we need to derive from (5) the Hamiltonian describing region 2 and determine the corresponding eigenvalues and eigenspinors. Then, we start from the eigenvalue equation $H_{\tau,2}\psi_2(x,y) = \epsilon\psi_2(x,y)$ with

$$H_{\tau,2} = \begin{pmatrix} v_0 + \mu + \frac{\tau}{2l_B^2} g\mu_0 & -i\left(\partial_x + k_y + \frac{x}{l_B^2}\right) \\ i\left(-\partial_x + k_y + \frac{x}{l_B^2}\right) & v_0 - \mu + \frac{\tau}{2l_B^2} g\mu_0 \end{pmatrix}, \qquad \psi_2(x,y) = (\varphi_1, \varphi_2)^T \tag{16}$$

where we have set the parameters $v_0 = V_0/\upsilon_F$, $\mu = t^{'}/\upsilon_F$, $\mu_0 = \mu_B/\upsilon_F$. Using all ingredients to obtain two dependent first order differential equations

$$\left(v_0 + \mu + \frac{\tau}{2l_B^2} g\mu_0\right)\varphi_1 - i\frac{\sqrt{2}}{l_B} a\varphi_2 = \epsilon\varphi_1 \tag{17}$$

$$i\frac{\sqrt{2}}{l_B} a^\dagger \varphi_1 + \left(v_0 - \mu + \frac{\tau}{2l_B^2} g\mu_0\right)\varphi_2 = \epsilon\varphi_2 \tag{18}$$

where the annihilation and creation operators are defined as

$$a = \frac{l_B}{\sqrt{2}}\left(\partial_x + k_y + \frac{x}{l_B^2}\right), \qquad a^\dagger = \frac{l_B}{\sqrt{2}}\left(-\partial_x + k_y + \frac{x}{l_B^2}\right) \tag{19}$$

which satisfy the commutation relation $\left[a, a^{\dagger}\right] = \mathbb{I}$. Now injecting (18) into (17) to find the second differential equation for φ_1

$$\left[\left(\epsilon - v_0 - \frac{\tau}{2l_B^2} g\mu_0\right)^2 - \mu^2\right] \varphi_1 = \frac{2}{l_B^2} a a^{\dagger} \varphi_1. \tag{20}$$

It is clear that φ_1 is an eigenstate of the number operator $\widehat{N} = a^{\dagger}a$ and therefore we identify φ_1 to the eigenstates of the harmonic oscillator $\mid n-1\rangle$, namely

$$\varphi_1 \sim \mid n-1\rangle \tag{21}$$

which gives the energy spectrum

$$\epsilon - v_0 - \frac{\tau}{2l_B^2} g\mu_0 = s_1 k_F = s_1 \frac{1}{l_B} \sqrt{(\mu l_B)^2 + 2n}. \tag{22}$$

The second spinor component can now be derived from (18) as

$$\varphi_2 = s_1 i \sqrt{\frac{k_F - s_1\mu}{k_F + s_1\mu}} \mid n\rangle \tag{23}$$

and therefore the corresponding eigenspinors, in terms of the parabolic cylinder functions

$$D_n(x) = 2^{-n/2} e^{\frac{-x^2}{4}} H_n\left(\frac{x}{\sqrt{2}}\right) \tag{24}$$

can be written as

$$\psi_2(x,y) = \frac{1}{\sqrt{2}} \begin{pmatrix} \digamma_{1,\tau} D_{((k_F l_B)^2 - (\mu l_B)^2)/2 - 1}\left[\pm\sqrt{2}\left(\frac{x}{l_B} + k_y l_B\right)\right] \\ \pm i s_1 \digamma_{2,\tau} D_{((k_F l_B)^2 - (\mu l_B)^2)/2}\left[\pm\sqrt{2}\left(\frac{x}{l_B} + k_y l_B\right)\right] \end{pmatrix} e^{\tau i k_y y} \tag{25}$$

where the parameters $\digamma_1$ and $\digamma_2$ are

$$\digamma_{1,\tau} = \sqrt{\frac{k_F + s_1\mu}{k_F}}, \qquad \digamma_{2,\tau} = \sqrt{\frac{2}{k_F l_B^2 (k_F + s_1\mu)}} \tag{26}$$

and $\epsilon - V = s_1 k_F$, $s_1 = \mathsf{sgn}\,(\epsilon - V)$ with $V = v_0 + \frac{\tau}{2l_B^2} g\mu_0$. The above $\pm$ signs stand for waves traveling to right and left, respectively, along the usual convention for the traveling waves $e^{\pm i k_x x}$ and $e^{\pm i k_{1x} x}$. The solution in region 2 is given by a linear combination, c^+ with the upper sign added to c^- with the lower sign. As usual the arbitrary coefficients $c^{\pm}$ can be determined using the boundary conditions, continuity of the eigenspinors at each interface. Next we will use the above solutions to compute the transmission coefficient as well as the associated phase shift and build a bridge between quantum optics and Dirac fermions in graphene.

3 Transmission and phase shift

Before determining explicitly the transmission coefficient and the phase shift, we notice that the total internal reflection will take place only when $0 < \phi < \frac{\pi}{2}$. This is because the wave incident from the

right- and left-hand sides of the surface normal will behave differently [22]. Then, we characterize our waves by introducing a critical angle ϕ_c defined by

$$\phi_c = \sin^{-1}\left[1 - \frac{d}{\epsilon l_B^2}\right]. \tag{27}$$

With this we can conclude that when the incident angle is less than ϕ_c, the modes become oscillating guided modes. However, in the case when the incident angle is more than ϕ_c, we have decaying or evanescent wave modes. In the forthcoming analysis, we will be interested in studying the situation where $\phi < \phi_c$.

To deal with our task, we proceed by using the continuity of the spinor wavefunctions at two interfaces $x = 0$ and $x = d$. These giving rise to a set of equations

$$1 + r_\tau = c^+ F_{1,\tau}\eta^+_{1,\tau} + c^- F_{1,\tau}\eta^-_{1,\tau} \tag{28}$$

$$\alpha - \frac{1}{\alpha} r_\tau = c^+ i s_1 F_{2,\tau}\xi^+_1 - c^- i s_1 F_{2,\tau}\xi^-_1 \tag{29}$$

$$c^+ F_{1,\tau}\eta^+_{2,\tau} + c^- F_{1,\tau}\eta^-_{2,\tau} = t_\tau e^{ik_{1x}d} \tag{30}$$

$$c^+ i s_1 F_{2,\tau}\xi^+_{2,\tau} - c^- i s_1 F_{2,\tau}\xi^-_{2,\tau} = \beta t_\tau e^{ik_{1x}d}. \tag{31}$$

After solving the system for the transmission amplitude t_τ, which is of interest to us, we can show that t_τ can be written in terms of the phase shift φ as

$$t_\tau = \frac{e^{i\varphi_\tau}}{f_\tau}. \tag{32}$$

Note that we have different reflection and transmission, which are depending on the nature of spin up or down. The function f_τ can be obtained from the relation

$$f_\tau e^{-i\varphi_\tau} = \frac{(A\cos\phi + B\sin\phi) + i\,(B\cos\phi - A\sin\phi)}{2F\cos\phi} e^{idk_{1x}} \tag{33}$$

where the shorthand notation are defined by

$$\begin{aligned} A &= sF^2_{1,\tau}\left(\eta^+_{1,\tau}\eta^-_{2,\tau} - \eta^-_{1,\tau}\eta^+_{2,\tau}\right)\sin\theta + sF^2_{2,\tau}\left(\xi^-_{1,\tau}\xi^+_{2,\tau} - \xi^+_{1,\tau}\xi^-_{2,\tau}\right)\sin\phi \\ &\quad + s_1 F_{1,\tau}F_{2,\tau}\left[\left(\eta^-_{1,\tau}\xi^+_{2,\tau} + \eta^+_{1,\tau}\xi^-_{2,\tau}\right) + \left(\eta^-_{2,\tau}\xi^+_{1,\tau} + \eta^+_{2,\tau}\xi^-_{1,\tau}\right)\cos(\theta+\phi)\right] \end{aligned} \tag{34}$$

$$\begin{aligned} B &= sF^2_{1,\tau}\left(\eta^-_{1,\tau}\eta^+_{2,\tau} - \eta^+_{1,\tau}\eta^-_{2,\tau}\right)\cos\theta + sF^2_{2,\tau}\left(\xi^+_{1,\tau}\xi^-_{2,\tau} - \xi^-_{1,\tau}\xi^+_{2,\tau}\right)\cos\phi \\ &\quad + s_1 F_{1,\tau}F_{2,\tau}\left(\eta^-_{2,\tau}\xi^+_{1,\tau} + \eta^+_{2,\tau}\xi^-_{1,\tau}\right)\sin(\theta+\phi) \end{aligned} \tag{35}$$

and we have set the quantities

$$\eta^\pm_{1,\tau} = D_{((k_f l_B)^2 - (\mu l_B)^2)/2 - 1}\left(\pm\sqrt{2}k_y l_B\right) \tag{36}$$

$$\xi^\pm_{1,\tau} = D_{((k_f l_B)^2 - (\mu l_B)^2)/2}\left(\pm\sqrt{2}k_y l_B\right) \tag{37}$$

$$\eta^\pm_{2,\tau} = D_{((k_f l_B)^2 - (\mu l_B)^2)/2 - 1}\left(\pm\sqrt{2}(\frac{d}{l_B} + k_y l_B)\right) \tag{38}$$

$$\xi^\pm_{2,\tau} = D_{((k_f l_B)^2 - (\mu l_B)^2)/2}\left(\pm\sqrt{2}(\frac{d}{l_B} + k_y l_B)\right) \tag{39}$$

$$F = s_1 F_1 F_2\left(\eta^+_{2,\tau}\xi^-_{2,\tau} + \eta^-_{2,\tau}\xi^+_{2,\tau}\right). \tag{40}$$

Actually from the above results, we can deduce the phase shift as

$$\varphi_\tau = -\arctan\left[\frac{B\cos(\phi - k_{1x}d) - A\sin(\phi - k_{1x}d)}{A\cos(\phi - k_{1x}d) + B\sin(\phi - k_{1x}d)}\right] \tag{41}$$

which can be used together with (33) to explicitly determine the transmission amplitude (32). This statement will be clarified in the forthcoming analysis.

Actually what we exactly need are the reflection R_τ and transmission T_τ coefficients corresponding to our system. These can be obtained by introducing the electric current density J corresponding to our system. Then from the previous Hamiltonian, we show that J takes the form

$$J = \pm i\upsilon_F \psi^\dagger \sigma_x \psi \tag{42}$$

which gives the incident, reflected and transmitted current components

$$J_{\mathsf{in}} = \upsilon_F(\alpha + \alpha^*) \tag{43}$$

$$J_{\mathsf{re},\tau} = \upsilon_F r_\tau^* r_\tau(\alpha + \alpha^*) \tag{44}$$

$$J_{\mathsf{tr},\tau} = \upsilon_F t_\tau^* t_\tau(\beta + \beta^*) \tag{45}$$

These can be used to define the reflection and transmission coefficients as

$$T_\tau = \frac{|J_{\mathsf{tr},\tau}|}{|J_{\mathsf{in}}|}, \qquad R_\tau = \frac{|J_{\mathsf{re},\tau}|}{|J_{\mathsf{in}}|} \tag{46}$$

where $T^\uparrow$ and $T^\downarrow$ have similar expression, the same applies to $R^\uparrow$ and $R^\downarrow$, but the only difference being that $\tau = 1$ instead of $\tau = -1$. After replacing, we obtain

$$T_\tau = \frac{k_{1x}}{k_x}|t_\tau|^2, \qquad R_\tau = |r_\tau|^2. \tag{47}$$

Combining all to express the transmission probability as

$$T_\tau = \frac{4k_{1x}F^2\cos^2\phi}{k_x\left(A^2 + B^2\right)}. \tag{48}$$

Obviously, we can check that the probability condition $T_\tau + R_\tau = 1$ is well satisfied. To under their behavior, let us consider Figure 2:

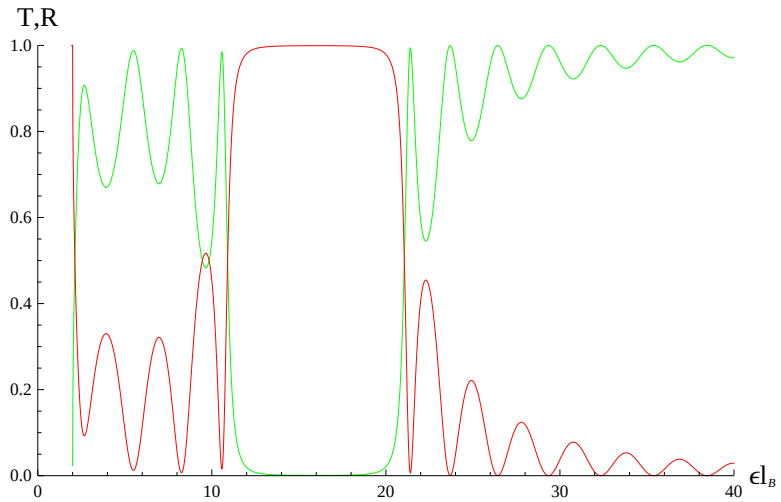

Figure 2: Transmission and reflection coefficients versus the energy ϵl_B for a single barrier with the parameters: $\mu_0 = 6l_B$, $d = 1l_B$, $v_0 = \frac{10}{l_B}$, $\mu = \frac{4}{l_B}$ and $k_y = \frac{1}{l_B}$.

Figure (2) presents the transmission (green line) and the reflection (red line) coefficients as function of the energy for $\mu_0 = 6l_B$, $d = 1l_B$, $v_0 = \frac{10}{l_B}$, $\mu = \frac{4}{l_B}$ and $k_y = \frac{1}{l_B}$. Clearly, it shows that there are different behaviors depending on the energy intervals. Indeed, in the first interval $\left(\epsilon l_B < k_y l_B + \frac{d}{l_B}\right)$ we have no transmission because there is a forbidden zone [23]. However, for the second interval $\left(k_y l_B + \frac{d}{l_B} < \epsilon l_B < v_0 l_B + \frac{1}{2l_B} g\mu_0 - \mu\right)$, there are oscillation resonances due to the Klein regime that is the situation in which only oscillatory solutions exist throughout and where the so called Klein paradox reigns [7]. We have no transmission (like a windows) when $v_0 l_B + \frac{1}{2l_B} g\mu_0 - \mu < \epsilon l_B < v_0 l_B + \frac{1}{2l_B} g\mu_0 + \mu$. Finally in the interval when $\epsilon l_B > v_0 l_B + \frac{1}{2l_B} g\mu_0 + \mu$ contains the usual high energy barrier oscillations and asymptotically goes to unity at high energy.

4 Goos-Hänchen like shifts

We begin our study of the Goos-Hänchen like (GHL) shifts by considering an incident, reflected and transmitted beams, at energy ϵ, around some transverse wave vector $k_y = k_{y0}$ corresponding to the central incidence angle ϕ_0 (see Figure 1), denoted by the subscript 0. These beams can be expressed in the integral forms as

$$\psi_{\mathsf{in}}(x,y) = \int_{\infty}^{\infty} dk_y A(k_y) e^{i(k_x(k_y)x + \tau k_y y)} \begin{pmatrix} 1 \\ s e^{i\phi(k_y)} \end{pmatrix} \tag{49}$$

$$\psi_{\mathsf{re}}(x,y) = \int_{\infty}^{\infty} dk_y r_\tau A(k_y) e^{i(-k_x(k_y)x + \tau k_y y)} \begin{pmatrix} 1 \\ -s e^{-i\phi(k_y)} \end{pmatrix} \tag{50}$$

$$\psi_{\mathsf{tr}}(x,y) = \int_{\infty}^{\infty} dk_y t_\tau A(k_y) e^{i(k_{1x}(k_y) + \tau k_y y)} \begin{pmatrix} 1 \\ s_1 e^{i\theta(k_y)} \end{pmatrix}. \tag{51}$$

The envelope function ensures the wavepacket is of finite size along the y-direction and is sharply peaked at $k_y = k_{y0}$. Therefore, we have the intervals $k_{y0} \in [0, \epsilon]$ and the angle of incidence $\phi(k_y) \in \left[0, \frac{\pi}{2}\right]$. This fact is represented by writing the x-component of wavevector k_x, k_{1x} as well as ϕ and θ all as function of k_y. $A(k_y)$is the angular-spectrum distribution around the central wave vector k_{y0}, which can be assumed of the Gaussian shape $w_y e^{-w_y^2(k_y - k_{y0})^2}$ with w_y being the half beam width at waist [14]. The reflection $r(k_y)$ and transmission $t(k_y)$ coefficients will be calculated through the use of boundary conditions. According to the stationary phase approximation [15], the GHL shifts of the transmitted beam through the graphene barrier can be defined as

$$s_t^\tau = -\frac{\partial \varphi_\tau}{\partial k_{y0}}. \tag{52}$$

We notice that the definition (52) can be applicable to any finite-width beam, not necessarily a Gaussian-shaped beam. According to (52), we need first to to determine the gradient of the phase φ_τ of the transmission coefficient. Because the expression of $s_t^\downarrow$ is similar to that of spin up, the only difference being that $\tau = 1$ instead of $\tau = -1$, then in the forthcoming analysis we focus only on $s_t^\uparrow$, which will simply be written as s_t.

To allow for a suitable interpretation of the GHL shift, we compute numerically s_t under various conditions. First we plot the GHL shifts as a function of energy for different parameters of our system considered in Figure 1 ($v_0 = 14/l_B$, $\mu_0 = 6l_B$, $d = 1.5l_B$ and $\tau = 1$) and three different values of the

incidence angle $\phi_1 = 4°, 6°, 8°$ with zero-gap $\mu = 0$ (Figure 3.a) and finite gap $\mu = 3/l_B$ (Figure 3.b). Obviously, it is clearly seen from Figure 3 that the GHL shifts, for graphene barrier in external magnetic field, can be negative as well as positive and change the sign near the point $\epsilon l_B = v_0 l_B + \frac{1}{2l_B} g\mu_0$, whereas after certain threshold energy value, which is compatible with a maximum of transmission, the GHL shifts become constant. Another most impressive behavior of the GHL shifts is that the position of the maximum or absolute value of s_t can be enhanced by the transmission resonances and related to the transmission gap, as observed in single and double barrier [15,17]. In addition to these properties, we notice that the absolute values of the GHL shifts are strongly dependent on the incidence angle, example of their independence is plotted with zero and finite gap. From Figure 3, we can show that the introduced gap influence the shifts. Then, it is also interesting to discuss the influence of the induced gap.

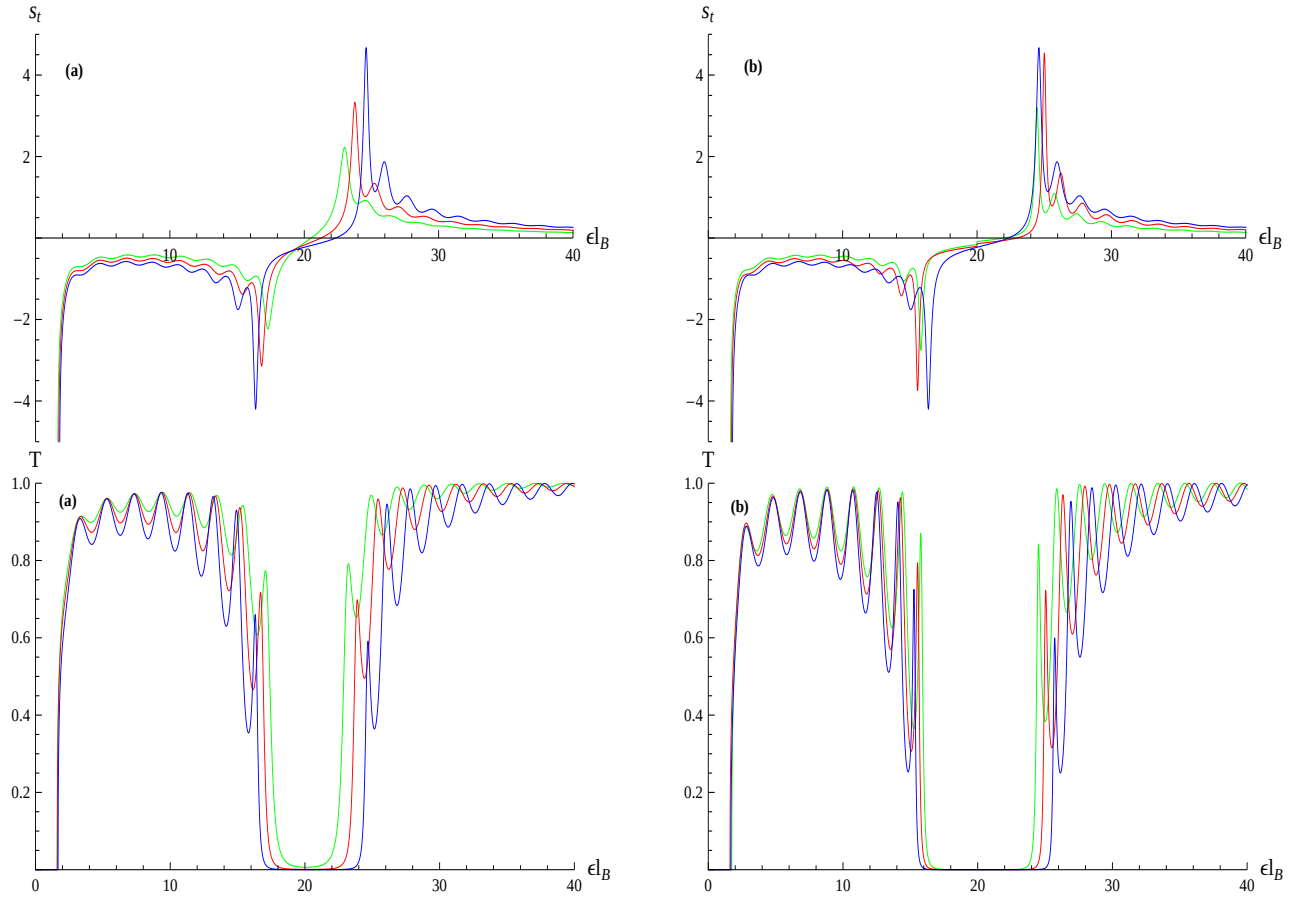

Figure 3: The GHL Shift and the transmission for graphene barrier in external magnetic field, as function of the energy(a)/(b), for $v_0 = \frac{14}{l_B}$, $\mu_0 = 6l_B$, $d = 1.5l_B$, $\tau = 1$, $(\mu = \frac{0}{l_B}, \phi = 4°)/(\mu = \frac{3}{l_B}, \phi = 4°)$ (Green line), $(\mu = \frac{0}{l_B}, \phi = 6°)/(\mu = \frac{3}{l_B}, \phi = 6°)$ (Red line), $(\mu = \frac{0}{l_B}, \phi = 8°)/(\mu = \frac{3}{l_B}, \phi = 8°)$ (Blue line).

Note that graphene is a zero gap semiconductor, despite these great properties suitable, its one of the biggest hurdles for graphene to be useful as an electronic material [24], however, to generate the energy gap is crucial for its application in making devices. There are two ways to generate the

energy gap in monolayer graphene, one requires breaking of the translational symmetry [25], the other is to break the equivalence between the A and B sublattice, which does not require any translation symmetry breaking [26–29]. These fascinating properties of graphene suggest to underline the behavior our findings with respect to the induced gap.

To answer above requirement, in Figure 4 we show the influence of the induced gap on the GHL shifts and the transmission as well. This has been performed by fixing the parameters $v_0 = \frac{15}{l_B}$, $\mu_0 = 6l_B$ and making different choices of the energy and the barrier's width. The GHL shifts become mostly constant up to some value then show sharp picks. It is found that the GHL shifts can be enhanced by a certain gap opening. In fact, we note that by increasing the gap, the gap of transmission become boarder that changing the transmission resonances, where the modulation of the GHL shifts. The dependence of the s_t on the barrier's width is shown in Figure 4. In addition, we mention that in the two configurations $\epsilon = \frac{12}{l_B}$, $d = 0.6l_B$ (Green line) and $\epsilon = \frac{12}{l_B}$, $d = 0.8l_B$ (Red line) where the condition $\epsilon l_B < v_0 l_B + \frac{1}{2l_B} g\mu_0$ is satisfied, the shifts is negative. However in the other two configurations $\epsilon = \frac{35}{l_B}$, $d = 0.6l_B$ (Blue line) and $\epsilon = \frac{35}{l_B}$, $d = 0.8l_B$ (Purple line) where $\epsilon l_B > v_0 l_B + \frac{1}{2l_B} g\mu_0$, the shifts is positive.

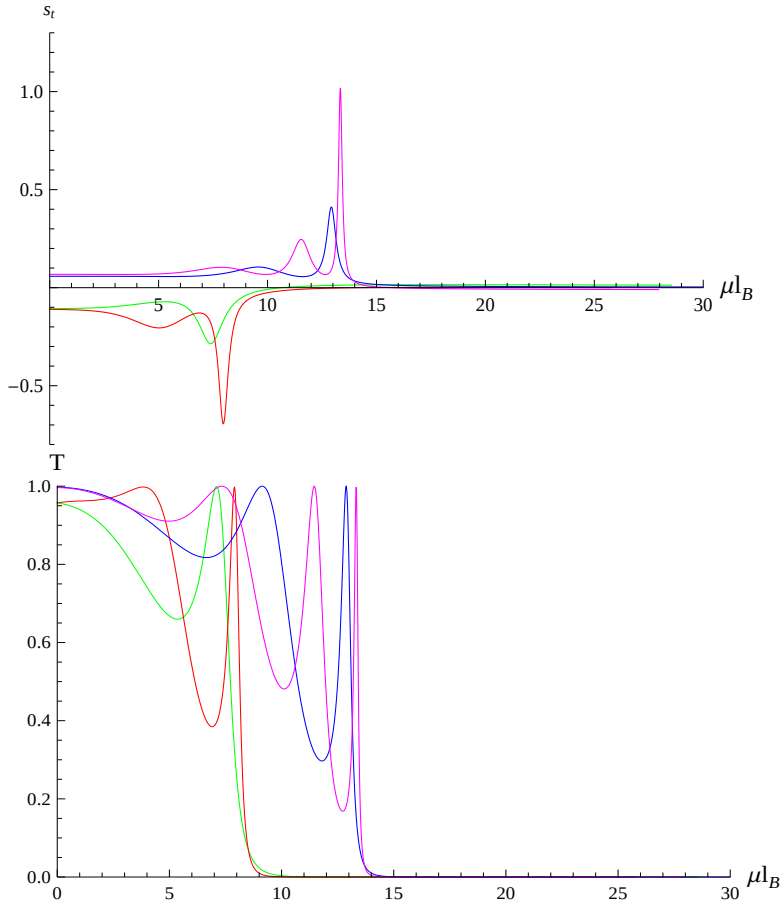

Figure 4: The influence of the induced gap on the GHL shifts and the transmission for graphene barrier in external magnetic field, for $v_0 = \frac{15}{l_B}$, $\mu_0 = 6l_B$, $k_y = 1$, $\tau = 1$, $\epsilon = \frac{12}{l_B}$, $d = 0.6l_B$ (Green line), $\epsilon = \frac{12}{l_B}$, $d = 0.8l_B$ (Red line), $\epsilon = \frac{35}{l_B}$, $d = 0.6l_B$ (Blue line), $\epsilon = \frac{35}{l_B}$, $d = 0.8l_B$ (Purple line).

Now let us investigate how the GHL shift behave as function of the barrier potential height that is represented numerically in Figure 5. We have fixed the parameters $\epsilon = \frac{15}{l_B}$, $\mu_0 = 6l_B$, $d = 1.5l_B$,$\mu = \frac{0}{l_B}$ and made different choices for the incidence angle $\phi = 4°, 6°, 8°$. It is clearly shown that the GHL shifts change their sign near the point $v_0 l_B = \epsilon l_B - \frac{1}{2l_B} g\mu_0$ and behave differently as compared to Figure 3. We notice that when the condition $v_0 l_B < \epsilon l_B - \frac{1}{2l_B} g\mu_0$ is fulfilled, the GHL shifts are positive, while negative when the height of the barrier satisfies the condition $v_0 l_B > \epsilon l_B - \frac{1}{2l_B} g\mu_0$. It is clearly seen from Figure 5 that the GHL shifts are strongly dependent on the barrier height V_0, which experimentally can be implemented by applying a local top gate voltage V_0 to graphene [30]. This tells us that the GHL shifts can be controlled by changing V_0.

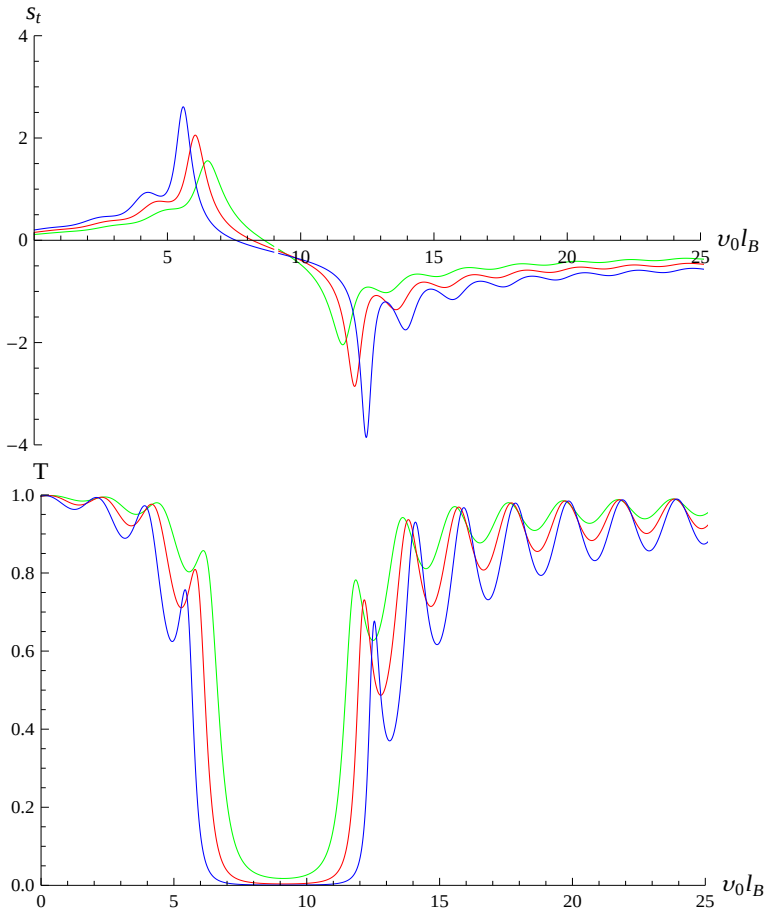

Figure 5: The GHL Shift and the transmission for graphene barrier in external magnetic field as function of the height of the potential barrier, for $\epsilon = \frac{15}{l_B}$, $\mu_0 = 6l_B$, $d = 1.5l_B$, $\tau = 1$,$\mu = \frac{0}{l_B}$, $\phi = 4°$ (Green line), $\phi = 6°$ (Red line), $\phi = 8°$ (Blue line).

In order to investigate what will happen when we change the value of the magnetic field, we plot the GHL shifts as function of the energy with different value of the magnetic field. The numerical results are shown in Figure 6 with the parameters $V_0 = 6meV$, $d = 1.5nm$, $t' = 2meV$, $\phi = 6°$ and different configurations of B ($0.9T$, $0.6T$, $0.4T$). We conclude that when we increase B the transmission gap become larger, the GHL shifts still change the sign, but the point of change of the sign moves to the left and the absolute value of the maximum of the shifts increase.

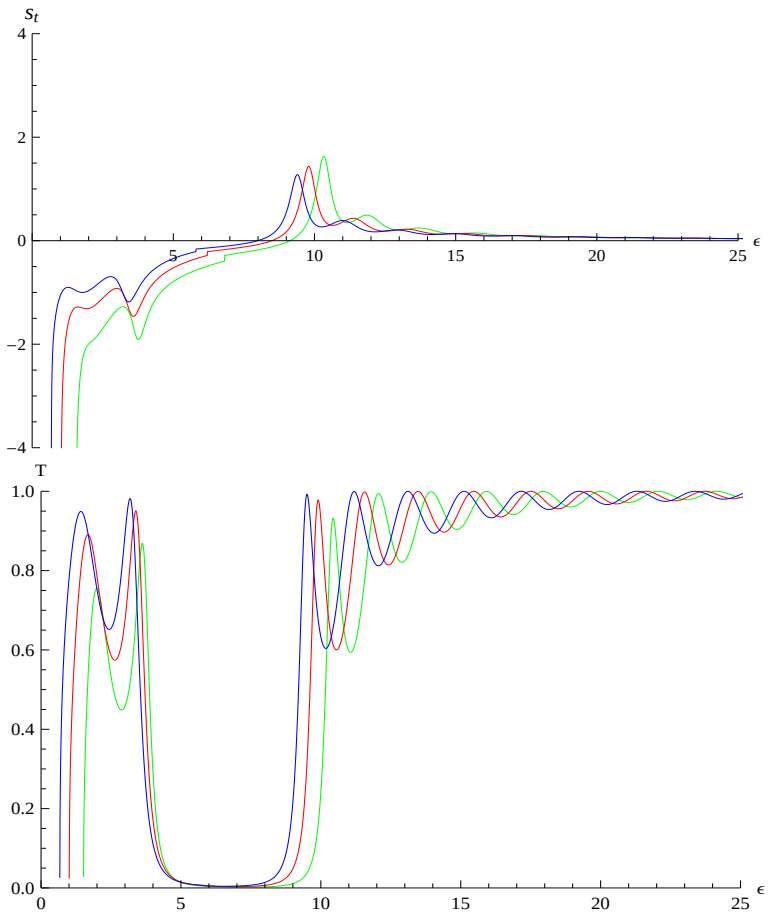

Figure 6: The GHL Shift and the transmission for graphene barrier in external magnetic field versus the energy, for $V_0 = 5meV$, $d = 1.5nm$, $t' = 2meV$, $\phi = 6°$ and $B = 0.9T$ (Green line), $B = 0.6T$ (Red line), $B = 0.4T$ (Blue line).

5 Conclusion

We have considered Dirac fermions in graphene with gap and submitted to a constant magnetic field as well as a barrier potential. By including Zeeman effect, the solutions of the energy spectrum were obtained to be dependent on various physical parameters. By matching the eigenspinors at interfaces we have calculated the transmission amplitude in terms of the phase shift φ_τ. These is used together with current density of our system to determine transmission and reflections probabilities. the transmission and reflections probabilities. Their behaviors were characterized by oscillating resonances for some interval of energy and forbidden zone where the reflection is total.

Subsequently, we have computed the Goos-Hänchen like shifts for graphene barrier in external magnetic field B. This has been done by considering an incident, reflected and transmitted beams, at energy ϵ, around some transverse wave vector $k_y = k_{y0}$ corresponding to the central incidence angle ϕ_0. We have given different plots of the shifts and the corresponding transmission coefficient versus different physical parameters. In fact, we have observed that there is a strong dependence of the GHL shifts on the incidence angle ϕ_0 (see Figure 1) and change as long as ϕ_0 changes. Also, the magnetic field affected the GHL shifts shifts because when B is increased, transmission gap became larger, the

GHL shifts still change the sign, but the point of change of the sign moved to the left and the absolute value of the maximum of the shifts increased as well. It was also observed that the transmission gap increased with the angle of incidence as long as it was less than the critical angle.

By comparing our results with those found for single and double barriers without B field [15–17], we have conclude that the common feature is that the GHL shifts can be positive as well as negative and can be enhanced by transmission resonances. Also the negative or positive shifts can be modulated by the height and width of potential barrier and the induced gap. These investigations allow to have potential application in various graphene based electronic devices.

Acknowledgment

The generous support provided by the Saudi Center for Theoretical Physics (SCTP) is highly appreciated by all authors.

References

[1] K. S. Novoselov, A. K. Geim, S. V. Morozov, D. Jiang, Y. Zhang, S. V. Dubonos, I. V. Grigorieva and A. A. Firsov, Science 306, 666 (2004).

[2] K. S. Novoselov, D. Jiang, T. Booth, V. V . Khotkevich, S. M. Morozov and A. K. Geim, Proc. Natl. Acad. Sci. 102, 10451 (2005).

[3] K. S. Novoselov, A. K. Geim, S. V. Morozov, D. Jiang, M. I. Katsnelson, I. V. Grigorieva, S. V. Dubonos and A. A. Firsov, Nature 438, 197 (2005).

[4] Y. Zhang, Y. W. Tan, H. L. Stormer and P. Kim, Nature 438, 201 (2005).

[5] G. W. Semenoff, Phys. Rev. Lett. 53, 2449 (1984).

[6] F. D. M. Haldane, Phys. Rev. Lett. 61, 2015 (1988).

[7] O. Klein, Z. Phys. 53, 157 (1929).

[8] C. Berger, Z. Song, X. Li, X. Wu, N. Brown, C. Naud, D. Mayou, T. Li, J. Hass, A. N. Marchenkov, E. H. Conrad, P. N. First and W. A. de Heer, Science 312, 1191 (2006).

[9] F. Goos and H. Hänchen, Ann. Phys. 436, 333 (1947).

[10] D. H. Foster, J. U. Nöckel and A. K. Cook, Opt. Lett. 32, 1764 (2007).

[11] N. H. Tran, L. Dutriaux, P. Balcou, A. Le Floch and F. Bretenaker, Opt. Lett. 20, 1233 (1995).

[12] L. Dutriaux, A. Le Floch and F. Bretenaker, J. Opt. Soc. Am. B 12, 2283 (1992).

[13] D. Q. Chowdhurry, D. H. Leach and R. K. Chang, J. Opt. Soc. Am. A 11, 1110 (1994).

[14] C. W. J. Beenakker, R. A. Sepkhanov, A. R. Akhmerov and J. Tworzydlo, Phys. Rev. Lett. 102, 146804 (2009).

[15] X. Chen, J.-W. Tao, and Y. Ban, Eur. Phys. J. B 79, 203 (2011).

[16] Y. Song, H-C. Wu and Y. Guo, Appl. Phys. Lett. 100, 253116 (2012).

[17] A. Jellal, I. Redouani, Y. Zahidi and H. Bahlouli, Physica E 58, 30 (2014).

[18] X. Chen, P-L. Zhao, X-J. Lu and L-G. Wang, Eur. Phys. J. B 86, 223 (2013).

[19] M. Sharma and S. J. Ghosh, Phys.: Condens. Matter 23, 055501 (2011).

[20] J. R. Williams, Tony Low, M. S. Lundstrom and C. M. Marcus, Nature Nanotechnology 6, 222 (2011).

[21] Y. Zhang, Z. Jiang, J. P. Small, M. S. Purewal, Y.-W. Tan, M. Fazlollahi, J. D. Chudow, J. A. Jaszczak, H. L. Stormer and P. Kim, Phys. Rev. Lett. 96, 136806 (2006).

[22] S. Ghosh and M. Sharma, J. Phys.: Condens. Matter 21, 292204 (2009).

[23] A. Jellal, E. B. Choubabib, H. Bahlouli and A. Aljaafari, J. Low Temp. Phys. 168, 51 (2012).

[24] S. Y. Zhou, G. H. Gweon, A. V. Federov, P. N. First, W. A. de Heer, D. H. Lee, F. Guinea, A. H. Castro Neto and A. Lanzara, Nat. Mater. 6, 770 (2007).

[25] J. L. Manes, F. Guinea and A. H. Vozmediano, Phys. Rev. B 75, 155424 (2007).

[26] B. Trauzettel, D. V. Bulaev, D. Loss and G. Burkard, Nature Phys. 3, 192 (2007).

[27] L. Brey and H. A. Fertig, Phys. Rev. B 73, 235411 (2006).

[28] Y. W. Son, M. L. Cohen, and S. G. Louie, Phys. Rev. Lett. 97, 216803 (2006).

[29] J. Nilsson, A. H. Castro Neto, F. Guinea and N. M. R. Peres, Phys. Rev. B 76, 165416 (2007).

[30] B. Huard, J. A. Sulpizio, N. Stander, K. Todd, B. Yang and D. Goldhaber-Gordon, Phys. Rev. Lett. 98, 236803 (2007).